17th World Conference on Earthquake Engineering, 17WCEE
Sendai, Japan - September 13th to 18th 2020

AN ALGORITHM TO ESTIMATE PHASE VELOCITY FROM AN ARRAY WITH ARBITRARY SHAPE USING MICROTREMOR DATA

H. Zhang[(1)], K. Iiyama[(2)], H. Morikawa[(3)]

[(1)] *Graduate Student, Tokyo Institute of Technology, zhang.h.aq@m.titech.ac.jp*
[(2)] *Assistant Professor, Tokyo Institute of Technology, iiyama.k.aa@m.titech.ac.jp*
[(3)] *Professor, Tokyo Institute of Technology, morikawa.h.aa@m.titech.ac.jp*

Abstract

Two methods have been generally recognized to calculate phase velocities, which are the frequency-wave number (F-K) spectral method and the spatial auto-correlation (SPAC) method. Although F-K method has no constraints on the shape of the array, the accuracy of results depends on the array shape. In addition, the SPAC method requires particular arrangement of the sensors, which can be difficult to realize in field observation. Attempts, such as Centerless Circular Array (CCA) method has been made to eliminate constraints on the shape of array. It can be applied to arbitrary array shape considering sensors spacing around a specific circle, but the determining process for which can be complex. Therefore, an algorithm of estimating phase velocity of Rayleigh wave using an arbitrary shape array is proposed.

On the basis of the analytical solution of Lamb's problem for vertical components of Rayleigh wave, the relationship between two observation points, p and q for example, is given in a discrete representation with the Bessel function of the first kind and higher-order Bessel functions, which is called Complex Coherence Function (CCF). Zhang and Morikawa extended the CCF to apply it to linear array situation. By adding an extra observation point s, the relationship between p and s can be expressed. For $kr_{max} \in [0, 5]$, where k and r_{max} stand for wave number and maximum distance between sensors on an array, respectively, Bessel functions of order greater than 6 can be ignored compared with lower-order Bessel functions' value. Hence, the CCF equations have only 5 unknowns left, including the phase velocity. We propose an algorithm to estimate the phase velocity using Artificial Bee Colony (ABC) algorithm under a constraint of $kr_{max} \in [0, 5]$.

For evaluating the accuracy of the proposed algorithm, numerical simulations were performed using five shapes of array arranged along an ellipse. Simulations were conducted 10 times by propagating 8 randomly generated wave sources with random power and directions. The results of proposed algorithm show that the estimation results match the theoretical value for frequency range from 0.25 Hz to 1.25 Hz for shapes 1 (regular shape), 2 (right-angled triangle) and 3 (obtuse triangle). However, for shapes 4 (near linear-array triangle) and 5 (linear array), the estimation results are relatively unsatisfactory. In addition, we applied SPAC method with same signals for shape 1 and applied CCA method (BIDO2.0 program of Cho) to shapes 1 to 4. The results show that the proposed algorithm can get almost same accuracy of SPAC method for shape 1. Comparing with CCA method, although the effective ranges are different, the proposed algorithm shows more stable results.

In conclusion, except for the near linear-array shape situation, the proposed algorithm is applicable to estimate the phase velocity of Rayleigh wave using arbitrary array shape.

Keywords: CCF, SPAC method, CCA method, arbitrary-shape array, phase velocity.

1. Introduction

Microtremor observation has been widely applied for estimating ground structure. Compared with traditional borehole drilling and logging method, microtremor array observation method is more cost-effective and mobile. Among those methods, two methods have been generally used for calculating phase velocity from the microtremor observed, which are the frequency-wave number (F-K) spectral method [1] and the spatial auto-correlation (SPAC) method [2].

Although F-K method doesn't have constraints on the array shape, it requires a rather larger number of sensors and the accuracy of results depends on the array shape. For the SPAC method, it requires fewer sensors than the F-K method but the sensors have to be arranged evenly on a circle to satisfy the azimuthal average condition. However, this can be difficult to realize for field observation. Attempts such as the direct estimation method (DEM) has been made to employ more flexible sensor arrangement but the overall arrangement has to be symmetric [3]. In addition, Centerless Circular Array (CCA) method [4] has been proposed to eliminate constraints on the shape of array. It can be applied to arbitrary array shape considering sensors spacing around a specific circle, but the determining process of the center can be complex. Also, it can't be applied to linear-array situation. Zhang and Morikawa [5] proposed a method and proved it to be applicable for linear array based on the SPAC method and complex coherence function (CCF) [6].

Therefore, we propose an algorithm based on the CCF to estimate phase velocity of Rayleigh wave using an arbitrary shape array. In this algorithm, Artificial Bee Colony (ABC) algorithm [7] is applied for solving the multi-dimensional equations encountered when conducting numerical simulations. Numerical simulations were performed for evaluating the accuracy of proposed algorithm. Furthermore, comparisons between this algorithm, the SPAC method and CCA method were conducted for certain array shapes.

2. Method

This section is devoted to introduce the derivation process of CCF. Analytical representations of a proposed algorithm which is based on CCF and suitable for arbitrary shape array will be discussed.

2.1 Complex Coherence Function

Away from a vertical point source, the vertical components of velocity on ground surface can be expressed by the analytical solution of Lamb's problem. Under the assumptions: 1) only the fundamental mode is dominant, and 2) different sources are not correlated, we introduce the discrete formula of the CCF between two observation points p and q, as shown in Fig.1, is expressed as

$$\gamma_{pq} = \sum_{l=1}^{L} \lambda_l \exp(-jkr\cos\theta_l), \quad (1)$$

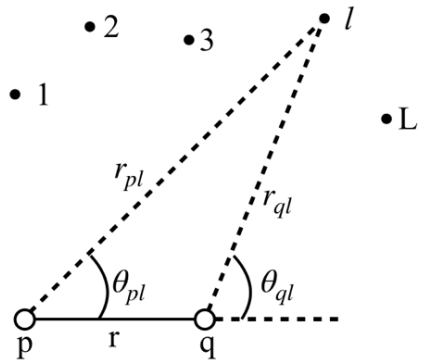

Fig. 1 – Geometry used in the formulation of complex coherence function (CCF) between observation points p and q.

where γ_{pq} denotes the CCF between observation points p and q. L denotes the total number of wave sources. λ_l is the contribution of wave source l to the power spectra at the observation point ($\sum_{l=1}^{L}\lambda_l = 1$). k is the wave number, and $k = \frac{2\pi f}{c}$, where c is phase velocity. r is the distance between receivers p and q. Here, $r_{pl} \approx r_{ql} \gg r_{pq}$, thus, $\theta_{pl} \approx \theta_{ql} \equiv \theta_l$.

With the relationship between cos ($xcos\theta$) and the Bessel function of the first kind, the real part of Eq. (1) can be expressed as [3]

$$Re(\gamma_{pq}) = J_0(kr) + 2\sum_{n=1}^{\infty}\{(-1)^n J_{2n}(kr)\sum_{l=1}^{L}\lambda_l cos2n\theta_l\}, \quad (2)$$

in which Re denotes the real part and J_n the n-th order Bessel function of the first kind.

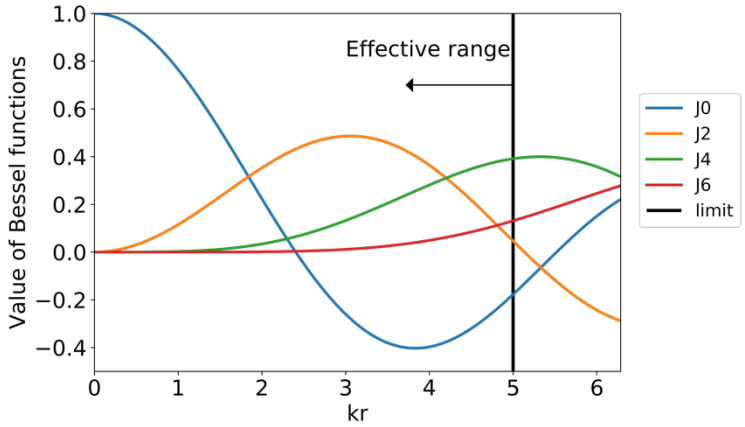

Fig. 2 – Value of J_0, J_2 , J_4 and J_6 with the effective range of $kr \leq 5$.

In the range of $kr \leq \pi$, $J_6(kr)$ and higher order Bessel functions are negligibly smaller than $J_0(kr)$ [3]. In fact, by comparing the values of Bessel functions of less than sixth-order as shown in Fig.2, this range can be extended to $kr \leq 5$. Thus, the real part of CCF can be reduced to J_0, J_2 and J_4 parts only as

$$Re(\gamma_{pq}) \approx J_0(kr) - 2J_2(kr)X_1 + 2J_4(kr)X_2, \quad (3)$$

where $X_1 \equiv \sum_{l=1}^{L}\lambda_l cos2\theta_l$ and $X_2 \equiv \sum_{l=1}^{L}\lambda_l cos4\theta_l$.

2.2 Extension of CCF for arbitrary shape array

By adding an observation point s anticlockwise α degree with respect to line pq from point p and with a distance of r_{ps}, we can get an arbitrary shape array consisting of three observation points p, q and s as in Fig.3 (a). From Eq. (3), we can get the real part of CCF between points p and s by replacing θ_l to $\theta_l - \alpha$, as shown in Eq. (4). Similarly, the real part of CCF between points q and s can be obtained by replacing θ_l to $\theta_l - \beta$, as in Eq. (5). Thus, for an array with 3 observation points, we can obtain 3 CCFs of Eq. (3), (4) and (5).

$$Re(\gamma_{ps}) \approx J_0(kr_{ps}) - 2J_2(kr_{ps})(X_1 cos2\alpha + Y_1 sin2\alpha) + 2J_4(kr_{ps})(X_2 cos4\alpha + Y_2 sin4\alpha) \quad (4)$$

$$Re(\gamma_{qs}) \approx J_0(kr_{qs}) - 2J_2(kr_{qs})(X_1 cos2\beta + Y_1 sin2\beta) + 2J_4(kr_{qs})(X_2 cos4\beta + Y_2 sin4\beta), \quad (5)$$

Here, $Y_1 \equiv \sum_{l=1}^{L}\lambda_l cos2\theta_l$ and $Y_2 \equiv \sum_{l=1}^{L}\lambda_l cos4\theta_l$. In Eq. (3) to Eq. (5), since we can obtain the left parts $Re(\gamma)$ from the observation records, there will be 5 unknowns left, including $c(k = \frac{2\pi f}{c})$, X_1, Y_1, X_2 and Y_2. Eventually, for this array with 3 observation points situation, our target changes to solve this problem with 3 equations and 5 unknows.

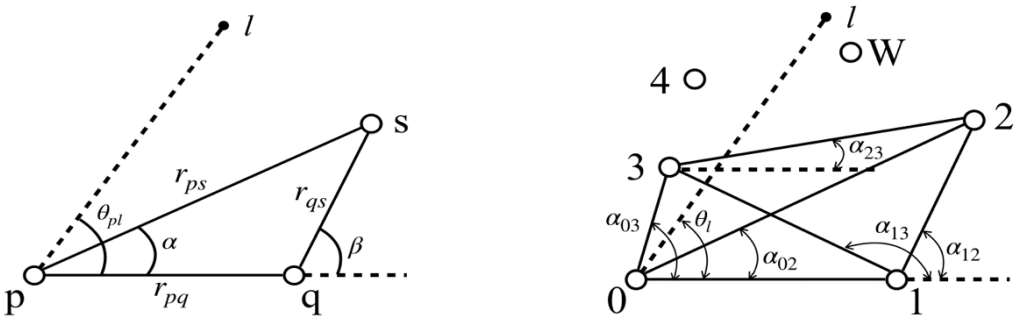

(a) Array with 3 observation points (b) Array with more than 3 observation points

Fig. 3 – Sensor arrangements for arbitrary shape arrays with 3 observation points and more than 3 observation points.

Furthermore, we can also extend the CCFs to the array with 4 and more observation points. If we denote the observation points from observation points 0 to M, as shown in Fig.3 (b), we can get $(M+1)$ observation points in total. Then the total number of CCFs becomes $\frac{M(M+1)}{2}$. The general expression of every CCF between each pair of observation points can be expressed as

$$Re(\gamma_{mn}) \approx J_0(kr_{mn}) - 2J_2(kr_{mn})(X_1 cos2\alpha_{mn} + Y_1 sin2\alpha_{mn}) + 2J_4(kr_{mn})(X_2 cos4\alpha_{mn} + Y_2 sin4\alpha_{mn}), \quad (6)$$

where m and n denote numbers of observation points, which are from 0 to M. r_{mn} denotes the distance between observation points m and n. And α_{mn} denotes the anticlockwise angle between the defined horizontal line, the 01 line here, and the mn line.

Although the total number of CCFs increases with increasing observation points, the unknowns remain the same, which are $c(k = \frac{2\pi f}{c})$, X_1, Y_1, X_2 and Y_2. That is to say, with increasing observation points, the number of CCFs will be greater than the unknowns' number 5. In that case, it is predictable that better results can be obtained because of the increased constraints.

In order to solve the multivariable problem, the ABC algorithm [7], which is an optimization algorithm based on the intelligent behavior of honey bee swarm, is applied. Since we want to optimize the results of $\frac{M(M+1)}{2}$ equations simultaneously, the fitness function is necessary. It is defined as

$$fitness = \frac{1}{N}\sum_{i=1}^{N} g_i^2, \quad (7)$$

where $N = \frac{M(M+1)}{2}$, the total number of the CCFs, and g_i is the difference of left side and right side of Eq. (6) for the i-th CCF.

2.3 Additional constraint condition

As mentioned in section 2.1, the effective range of phase velocity is $kr \leq 5$, where $k = 2\pi f/c$. For the numerical simulations, the results are reliable only if this condition is satisfied. Therefore, we add a constraint process during the optimization process and the flow chart is shown in Fig.4.

After every searching cycle, we can get a results vector consisting 50 sets of optimized variables. Then we get all of the local minimums and global minimum from the results vector. Next, check if the global minimum relative phase velocity satisfies the condition $kr_{max} \leq 5$, where r_{max} is the maximum distance among all of the observation points. If the condition is not satisfied, we will delete this global minimum and move to the next global minimum of the renewed results vector. After that, repeat this process until the global minimum satisfies the condition.

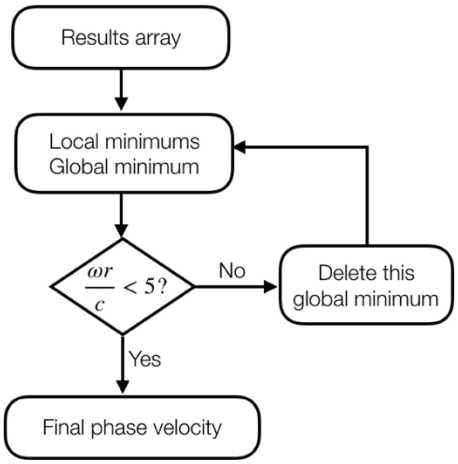

Fig. 4 – Flow chart of the constraint process applied during the optimization process.

3. Numerical Simulations

In this section, numerical simulations of arrays with 3 observation points were carried out to testify the validity of the proposed constraint condition. Also, the applicability of the proposed algorithm to arrays with arbitrary shape will be discussed. Furthermore, numerical simulations of the conventional methods, the SPAC method and the CCA method, were conducted with same signals. The results of the above simulations will be discussed.

3.1 Problem settings

To conduct numerical simulations, five arrays of different shape were designed as shown in Fig.5. All of the triangles are on the same ellipse with observation points 0 and 1 being their focuses and the moving observation point 2 being their top vertex. Here, observation points 0 and 1 are fixed with a distance of 100 meters. Among these shapes, shape 1 is a regular triangle, which was designed for comparing the proposed algorithm with the SPAC method and the CCA method (BIDO2.0 program of Cho) [8]. Shape 2 (right-angled triangle), shape 3 (obtuse triangle) and shape 4 (near linear-array triangle) will be used for the proposed algorithm and the CCA method. And the last shape, shape 5 (linear array), will be tested for the proposed algorithm only.

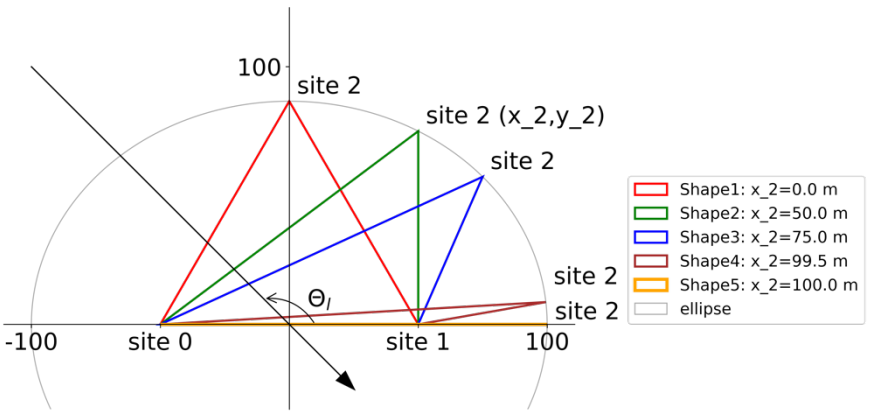

Fig. 5 – Array settings used for numerical simulations.

For the wave sources, 10 sets of 8 randomly generated wave sources were used for every shape. Every source's wave direction, θ_l, is randomly selected from set $\{\frac{\pi}{18}, \frac{2\pi}{18}, \ldots, \frac{35\pi}{18}, 2\pi\}$. And the power spectral density (PSD) function is

$$f(x) = \begin{cases} A \cdot \left| sin \frac{2\pi f}{D} \right|, & 0 < f \leq 10\ Hz \\ 0, & 10\ Hz < f \leq 50Hz \end{cases} \tag{8}$$

where A is the amplitude randomly selected from set {1,2,4,8}. And D is the denominator that randomly chosen from set {2,4,5,8,10}. Fig.6 shows an example of PSD generated for a wave source in a case of A = 8 and D = 5.

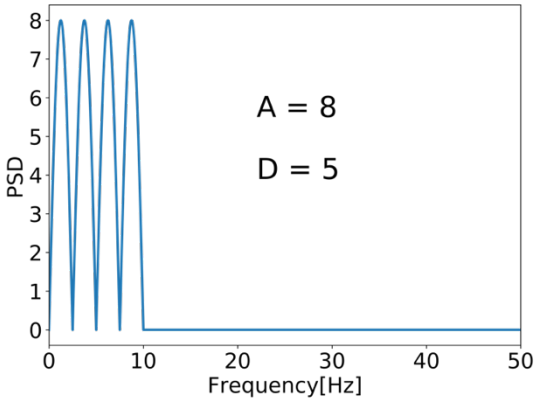

Fig. 6 – An example of randomly generated PSD of one source.

For settings of the constraint condition, considering the constraint $kr_{max} \leq 5$, the defined dispersion curve $c = \frac{0.6}{f+1} km/s$ and the relationship $k = \frac{2\pi f}{c}$, the effective range of frequency changes with r_{max}. r_{max} is the maximum distance among r_{mn}, $0 \leq m, n \leq M$. Since $100 \leq r_{max} \leq 150$ for all of the shapes, the maximum effective frequency f_{max} varies from 1.74 Hz to 1.35 Hz. For this reason, we will discuss the results which are within 2.0 Hz range.

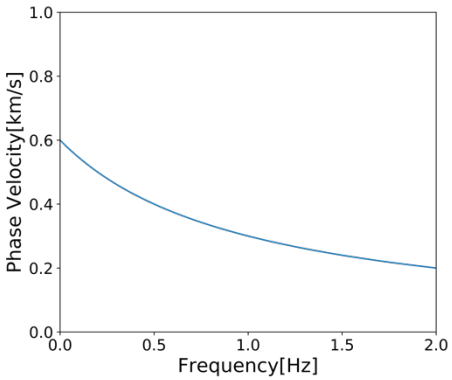

Fig. 7 – The defined dispersion curve, $c = \frac{0.6}{f+1} km/s$, for numerical simulation.

As for the ABC algorithm, the searching range for the first unknown variable c, phase velocity, is $0 < c < 1\ km/s$. This searching range was selected from the defined dispersion curve, the expression equation of which is $c = \frac{0.6}{f+1} km/s$, as shown in Fig.7. For other unknown parameters, X_1, Y_1, X_2 and Y_2, considering $-1 \leq \cos(n\theta_l) \leq 1$, $0 < \lambda_l \leq 1$ and $\sum_{l=1}^{L} \lambda_l = 1$, their searching range should be $[-1, 1]$. In addition, the number of food sources are set as 50 and the maximum cycle number for one optimization is 1000 here.

3.2 Confirmation of the effect of the constraint condition

Before the numerical simulations of sets of wave sources, simulations of one wave source were conducted. However, without the constraint, the results were not satisfactory since the ABC algorithm can get fluctuated

rather than smooth dispersion curves. Even for the regular triangle shape, shape 1, the calculated dispersion curve got large fluctuations with wave sources of certain directions. As shown in Fig.8, the blue line represents the original results of the regular triangle array without constraint process, which is proposed in section 2.3. There were sudden changes of the dispersion curve for frequency range from around 0.75 Hz to 1.0 Hz.

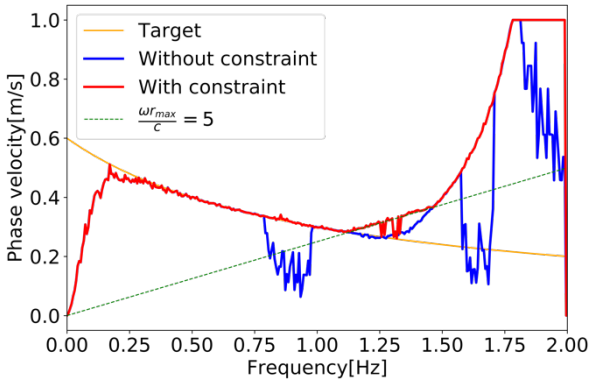

Fig. 8 – One example of the effect of constraint condition.

By checking the global minimums and local minimums of every cycle, we found that the ABC algorithm reached another local minimum as the final result. But for most of the situations, the relative ideal global minimum is still in the results vector, which means that we can pick it out by adding the constraint process as mentioned in section 2.3. After the constraint process, the sudden fluctuations disappeared and the resultsof frequency range less than 1.1 Hz is quite accurate, as shown in Fig.8. It can be seen that after applying the constraint condition, the effective range changes from $[0.25\ Hz, 0.75\ Hz]\ and\ [1.00\ Hz, 1.25\ Hz]$ to continuous $[0.25\ Hz, 1.1\ Hz]$. This confirms the effectiveness of the proposed constraint condition and the applicability of this proposed algorithm to arrays with irregular shapes.

3.3 Applicability to array with irregular shapes

For every shape, 10 sets of wave sources were generated for the simulation. In addition, the proposed algorithm will repeat 10 times for every set of wave sources. The respective results of every shape are shown in Fig.9 and the whole averaged results of 10 sets of wave sources are shown in Fig.10.

In case of the regular triangle, right-angled triangle and obtuse triangle (Fig.9 (a), (b) and (c)), the estimation results of the proposed algorithm match the defined dispersion curve, black solid line (labeled 'Target') for frequency range 0.25 Hz to 1.25 Hz. But the estimation results are poor for near linear-array triangle and linear array (Fig.9 (d) and (e)). Moreover, the shape of the constraint line, $kr_{max} \leq 5$ (the black dotted lines), becomes more obvious for these two shapes. The constraint condition works successfully for relative regular shapes without showing obvious constraint lines, but when it comes to near linear-array shapes, because of larger fluctuations of the estimation results, the constraint effects become clearer.

Although large deviations can be seen from the results, the averaged results in Fig.10 show a tendency of approaching the defined dispersion curve, especially shape 5. This suggests that when applying the proposed algorithm to field observations, for irregular shapes that are closer to linear shape, longer duration might be necessary to get accurate phase velocity.

Also, it is strange that the near linear-array triangle's averaged results are better than the linear array's results. However, the deviation of shape 4 is obviously smaller than shape 5. The causes of this might include the generated wave sources' difference, just the coincidence of averaging and so on, which can be a theme of future works.

To conclude, the numerical simulation results confirmed the availability of proposed algorithm for array shapes that are not near linear-array situations. As for near linear-array situations, relative accurate results might be get by increasing the observation time.

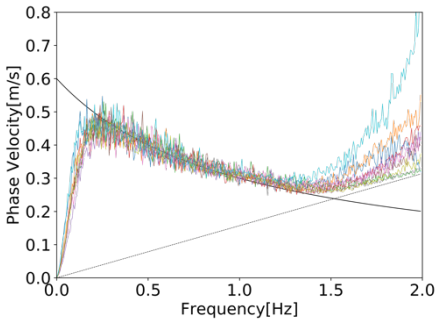

(a) Shape 1, regular triangle

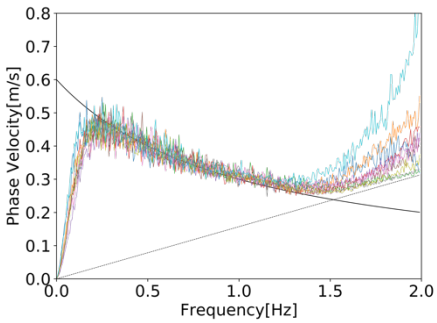

(b) Shape 2, right-angled triangle

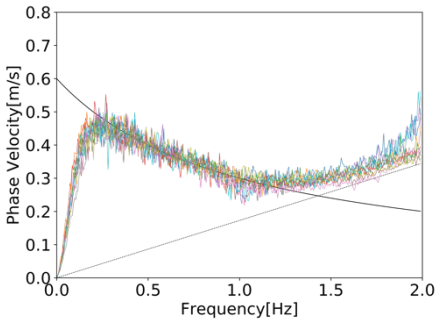

(c) Shape 3, obtuse triangle

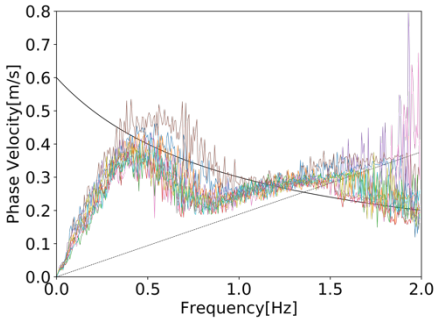

(d) Shape 4, near linear-array triangle

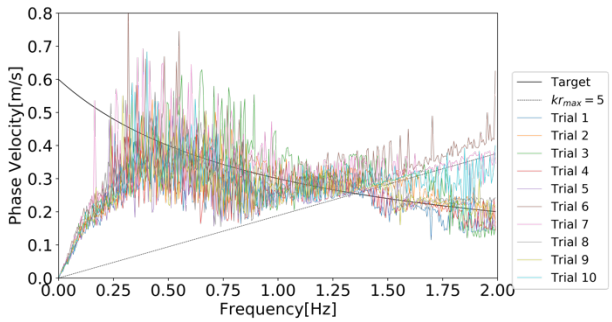

(e) Shape 5, linear array

Fig. 9 – The phase velocity results of 10 sets of wave sources for five array shapes

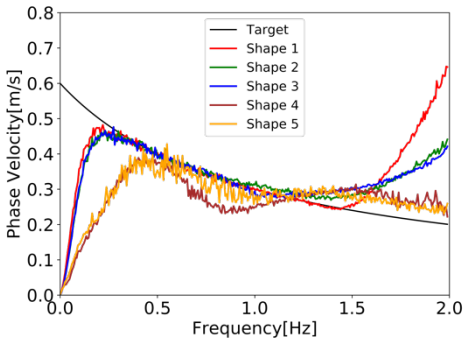

Fig. 10 – The average phase velocity result of 10 sets of wave sources.

3.4 Comparison with the conventional methods

Numerical simulations of SPAC method, shape 1 only, and CCA method, shape 1 to shape 4, were conducted with same signals as used in the previous section. For comparison, the results of the SPAC method, the CCA method and the proposed algorithm (labeled 'CCF with ABC') are all shown in one figure for every shape as shown in Fig.11.

In the case of regular triangle, as shown in Fig.11 (a), proposed method got almost same effective range and accuracy with the SPAC method. The effective range is around 0.25 Hz to 1.35 Hz. As for the CCA method, it is more accurate for the lower frequency range, around 0 Hz to 0.85 Hz, but with larger standard deviations. Similar characteristics can be found for the right-angled shape (shape 2) and obtuse triangle (shape 3). However, the effective range of both the CCA method and the proposed method narrow with the array shape more irregular (or near linear-array shape). Inevitably, when it comes to the near linear-array shape (shape 4), the CCA's effective range narrows to around $[0.05\ Hz, 0.25\ Hz]$ and the proposed method narrows to $[0.35\ Hz, 0.6\ Hz]$ with an unsatisfactory mean values and larger standard deviations.

Compared with the SPAC and the CCA methods, the proposed method can be applied to array with more irregular shapes. But for the lower frequency range, especially from 0.0 Hz to 0.25 Hz, the proposed method can't get closer results for any shapes of arrays. It suggests that a combination of the CCA method and the proposed method will give better results with wider range and less restrictions of the shapes of array shapes.

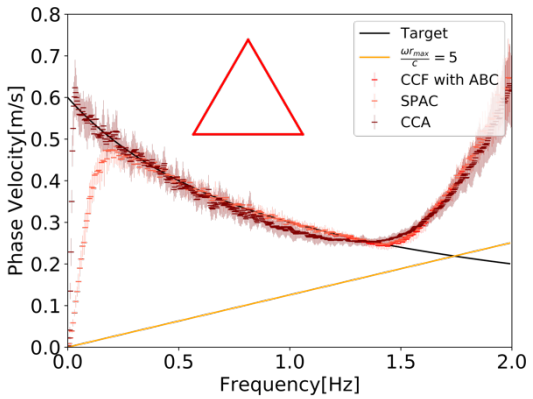

(a) Shape 1, SPAC, CCA and proposed algorithm

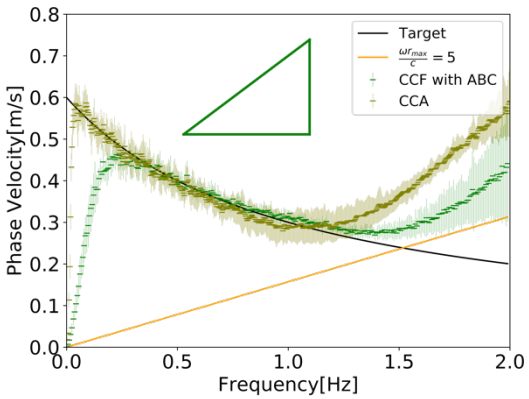

(b) Shape 2, CCA and proposed algorithm

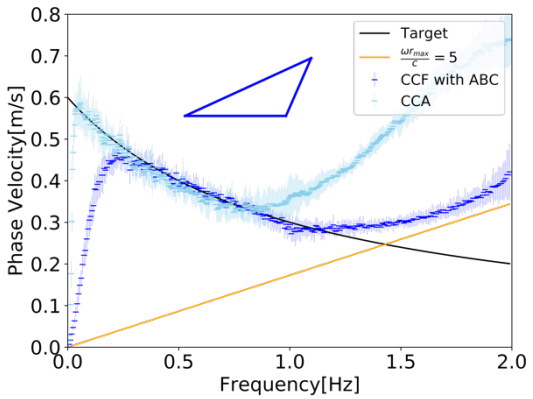

(c) Shape 3, CCA and proposed algorithm

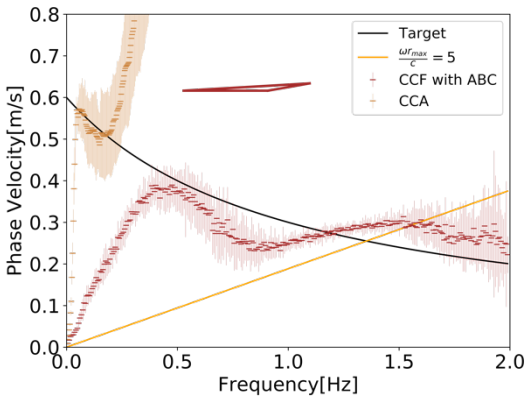

(d) Shape 4, CCA and proposed algorithm

Fig. 11 – Estimation results of the SPAC method, the CCA method and the proposed algorithm, CCF with ABC algorithm.

4. Conclusion

We proposed a new algorithm to estimate phase velocity of Rayleigh wave using an arbitrary shape array. This algorithm is based on the extension of CCF and the multivariable optimization algorithm, ABC algorithm. Also, a constraint condition, $kr_{max} \leq 5$, is proposed to reduce the fluctuations of the results.

To confirm the validity of the proposed algorithm, numerical simulations were conducted for five shapes, including regular triangle, right-angled triangle, obtuse triangle, near linear-array triangle and a linear array. The constraint process was proved effective for both one-source and multi-source wave fields.

In conclusion, the numerical simulation results confirmed the availability of proposed algorithm for array shapes that are not near linear-array situations. Also, relative accurate results might be get by increasing the observation time for near linear-array situations. Still, for near linear-array shapes and linear array shape, the proposed algorithm's accuracy is not satisfactory and needs further improvement. And a combination of the CCA method and the proposed method is suggested to get better results with wider range of frequency and less restrictions of the shapes of array shapes. In summary, we think the proposed algorithm can be applied for field observations with a more free arrangements of array.

For future works, we want to study the causes of strange averaged results as mentioned in section 3.3 and the limits of arrays with 3 observation points. The accuracy and arrangements of array shapes for arrays with 4 and more observation points can also be part of the future works. And the filed test of the proposed method will be conducted later.

5. Acknowledgements

A part of this work is supported by JSPS KAKENHI Grant Numbers JP19H02400 and JP17H02064.

6. References

[1] Capon J (1969): High-resolution frequency-wavenumber spectrum analysis. *Proceedings of the IEEE*, **57**(8), 1408-1418.

[2] Aki K (1957): Space and time spectra of stationary stochastic waves, with special reference to microtremors. *Bulletin of the Earthquake Research Institute, University of Tokyo*, **35**(3), 415-456.

[3] Shiraishi H, Matsuoka T, Asanuma H (2006): Direct estimation of the Rayleigh wave phase velocity in microtremors. *Geophysical research letters*, **33**(18).

[4] Cho I, Tada T, Shinozaki Y (2006): Centerless circular array method: Inferring phase velocities of Rayleigh waves in broad wavelength ranges using microtremor records. *Journal of Geophysical Research: Solid Earth*, **111**(B9).

[5] Zhang X, Morikawa H (2015): Discussion on Using Only One Linear Array to Estimate the Phase Velocity of Rayleigh Wave Based on Microtremor Survey. *British Journal of Applied Science & Technology*, **6**(4), 350.

[6] Shiraishi H, Matsuoka T, Asanuma H (2006): Direct estimation of the Rayleigh wave phase velocity in microtremors. *Geophysical research letters*, **33**(18).

[7] Karaboga D, Basturk B (2007): A powerful and efficient algorithm for numerical function optimization: artificial bee colony (ABC) algorithm. *Journal of global optimization*, **39**(3), 459-471.

[8] Cho I. (2010). BIDO Version 2.0, https://staff.aist.go.jp/ikuo-chou/BIDO/2.0/bidodl.html (accessed Aug. 26, 2019).

